Reactive PLIF method for characterisation of Micromixing in Continuous High-Throughput Chemical Reactors

João Peres Ribeiro[(a)], Margarida S.C. A. Brito[(b),(c)], Ricardo Jorge Santos[(b),(c)], Maria Isabel Nunes[(a)]*

(a) CESAM - Centre for Environmental and Marine Studies – Associated Laboratory, Department of Environment and Planning, University of Aveiro, Campus Universitário de Santiago 3810-193 Aveiro, Portugal
(b) LSRE-LCM – Laboratory of Separation and Reaction Engineering – Laboratory of Catalysis and Materials, Faculty of Engineering, University of Porto, Rua Dr. Roberto Frias, 4200-465 Porto, Portugal
(c) ALiCE – Associate Laboratory in Chemical Engineering, Faculty of Engineering, University of Porto, Rua Dr. Roberto Frias, 4200-465 Porto, Portugal
* Correspondence: isanunes@ua.pt

Abstract: This work aims to test and optimise reactive Planar Laser Induced Fluorescence (PLIF) methods for visualisation of the micromixing regions in chemical reactors using standard PLIF and Particle Image Velocimetry (PIV) equipment with laser source 512 nm. Two methods were tested: (i) an acid-base reaction with fluorescein as the reaction sensitive tracer and (ii) the Fenton's reaction, with rhodamine-B as the reaction tracer. Both test-reactions were studied in a stopped-flow equipment to define suitable operational conditions, namely chemical composition of the inflow streams, concentration of reagents and fluorophore, and suitable excitation light wavelength. The visualization of the micomixing regions was tested in a continuous flow reactor with a T-jets geometry. A laser light sheet emitted from an Nd:YAG laser illuminated the axial section of the demonstration reactor. The mixing dynamics and the reaction course were clearly visualised from the acid-base reactive PLIF images. Fenton reactive PLIF method showed the overall distribution of mixing and reaction regions. The main contribution of this work is benchmarking two methods with costs that enable the visualization of micromixing regions in continuous high-throughput reactors.

Keywords: micromixing; test-reactions; fluorescein; rhodamine-B; PLIF; T-Jets mixer

1. Introduction

Mixing has a significant impact on the performance of chemical reactors, because reactions occur from the contact between reagents [1]. Mixing can be the limiting factor for industrial processes such as combustion reactions or biological initiation processes [2] and its effect is especially evident in the scaling up equipment that involves chemical reactions [1, 3].

Micromixing can be assessed from physical and chemical methods. Physical methods are based on the incorporation of a non-reactive tracer in the fluid streams and either: (a) measurement of its concentration at different locations, including reactor outlet, as a function of time (e.g. Nadeau et al. [4]) or (b) visualisation of pathlines inside the reactor by optical methods (e.g. Buchmann and Mewes [5], Buchmann and Mewes [6]). Thus, while the physical methods are related to the degree of the homogeneity of the fluid, chemical methods are based on test-reactions, where product yield or reagent consumption are used to monitor reaction course and infer micromixing degree. Test-reactions with specific characteristics are used as chemical probes [7, 8] enabling quantities as the selectivity of a competitive reaction or a micromixing time, which are related with the degree of micromixing but give no information on its relation with the flow structure.

Table 1 and Table 2 summarise the methods, published in the last 30 years, for quantitatively studying micromixing based on competitive-consecutive and competitive-parallel reactions, respectively. All test-reactions have strong and weak points, as thoroughly discussed in the references cited across Table 1 and 2.

In recent years, another family of chemical methods for the assessment of the micromixing has gained importance in the literature. These methods are based on the optical

visualisation of the mixing process, allowing the quantitative measurement or assessment of mixing. Amongst them, there are two main types of optical methods suitable for this purpose: fluorescence-based techniques, particularly LIF (Laser Induced Fluorescence) and chemiluminescence-based techniques.

LIF experiments were introduced as a flow visualisation technique in the 70s by Dewey [9], Owen [10] and Liu et al. [11]. This technique consists of injecting a fluorescent tracer into the flow which will be excited by a laser. The dye absorbs the energy emitted by the laser and then re-emits a portion of that energy as fluorescence. Fluorescence can be optically measured and used to determine mixing in a section of a flow [1].

Tracer is typically an organic fluorescent dye soluble in water. Fluorescein and rhodamine (Rhodamine 6G and Rhodamine B) are the most common LIF dyes. Fluorescein (a.k.a. uranine or disodium acid) is particularly sensitive to pH [12]. Rhodamine B (a.k.a. Rhodamine 610) [13, 14], Rhodamine 6G (a.k.a. Rhodamine 590) [15, 16] and Rhodamine-WT [17] are relatively insensitive to pH, whereas the temperature sensibility was reported by Sakakibara et al. [18], Kuzkova et al. [19]. The PLIF using non-reactive tracers has been different applications, such as for the measurement of temperature fields in a gas-stirred ladle [20], the study of the coolant mixing in reactor vessel down-comer [21] and the interphase mass transfer of immiscible liquid-liquid system in a stirred tank [22], the measurement of solute-induced Marangoni effect of a growing drop Wang et al. [23] and the characterization of mixing efficiency in particle-laden Taylor-Couette flows [24].

In this work, fluorescein and rhodamine B (RhB) are the two selected tracers in reactive LIF experiments. Fluorescein is used as a marker in an acid-base reaction because its fluorescence is sensitive to the pH of the reaction medium. Variations in fluorescence will identify the pH changes in the reaction course. Differences in the fluorescence emission enable the tracking of the reactive fronts, which correspond to the regions controlled by the small-scale mixing, mainly at the molecular scale (micromixing). This method is named in this work as AB-RPLIF. Although AB-RPLIF is best with 488 nm laser equipment, here the method is tuned for the widespread Nd:YAG laser @532 that ships with most PIV/PLIF commercial equipment, but are better adjusted for the RhB methods.

A second reaction using RhB is also tested in this work. A redox reaction system will promote the oxidation of RhB organic tracer, and the variation of emission wavelength. This reaction will enable the quantification the visualization of micromixing by the disappearance of tracer in the reaction zones. This method is referred hereafter as Oxi-RPLIF.

Tests on the performance of these two tracers will contribute to the implementation of reactive LIF technique on micromixing visulaizaiton studies in continuous reactors with industrial applications, such as in opposed jets mixers. The performance of the two techniques is benchmarked in T-Jet mixers. Literature also reports other works for other reactors using AB-RPLIF [25-27] and Oxi-RPLIF [28-30].

The goal of this work is to test and optimise two luminescence methods to visually characterise the space-time dynamics of micromixing in chemical reactors. The replacement of one of the reagents to improve reaction usability and the validation of these methods in T-jets micromixing assessment are novel features of this work. The principle of both methods is similar and based on the emission intensity measurement of a fluorescent marker included in the reactional medium. The methods addressed in this work have been previously addressed in the literature as LIF methods to replace more established methods.

Table 1. Operational parameters for several chemical methods for assessing micromixing, based on competitive-consecutive reactions A + B → R; R + B → S.

Reagent A	**Reagent B**	**Kinetic rate constant (25 ºC)** [$m^3 \cdot mol^{-1} \cdot s^{-1}$]	**Reference**	**Analytical Method**
1- and 2-naphtol (A1 and A2)	Diazotised sulphanilic acid	k_1 = 1.3 x 10^4; k_2 = 2.7	Bourne [31], Bourne et al. [32] Nunes et al. [33]	A_1 + B → R B + R → S A_2 + B → Q B is the limiting reagent and A is buffered to pH=9.9 (usually Na_2CO_3/$NaHCO_3$); Absorption Spectrophotometry technique used for measurement of the products over time, at λ_{max}, which are 510 nm for R, 560 nm for S and 480 nm for Q;
Alkaline solution of $BaCl_2$, NaOH, Na_2SO_4 and EDTA	HCl	k_1 = 1.8 x 10^8 k_2=not reported	Barthole et al. (1982), in Meyer et al. [34]	Absorption Spectrophotometry technique. Mixing of the reagents takes place in stirred tanks. After the injection of B into A, a representative sample is taken and absorbance of precipitate product BaSO4 is measured at 650nm
1,3,5 - Trimetoxybenzene (TMB)	Bromine	$k_1/k_2 \approx 27$	Bourne and Kozicki [35] Bourne [31] and Hecht et al. [36]	High performance liquid chromatography technique. TMB and bromine flow from different streams and downstream from the mixer (different types of mixer tested), an HPLC device is used to analyse the products, separating TMB, product R and product S
Mo^- as $(NH_4)_2MoO_4$	Ti^{2+} (tiron as disodium salt)		Oates and Harvey [37] Zhang et al. [38]	Absorption spectrophotometry and absorbance imaging techniques. Absorbance at 580 nm was measured in samples taken downstream from the mixer. Additionally, polychromatic absorbance was measured in a glass mixing chamber by means of a CCD camera. Then the absorbance over the visual spectrum, which is what the digital camera observes, was compared to the absorbance at 580 nm

Table 2. Operational parameters for several chemical methods for assessing micromixing based on competitive-parallel reactions: A + B → R; C + B → S.

Reagent A	**Reagent B**	**Reagent C**	**Kinetic rate constant (25 ºC)** [$m^3 \cdot mol^{-1} \cdot s^{-1}$]	**Reference**	**Analytical Method**
Hydrochloric acid	Sodium hydroxide	Ethyl monochloroacetate	k_1 = 1.3-1.4 × 10^8; k_2 = 0.023-0.031	Akiti [39] Bourne [31], Baldyga et al. [40], Bałdyga et al. [41], Bourne and Yu [42]	Chromatographic analysis. Reagents A and C are premixed in a mixing vessel and then B is added. Samples are taken from the stirred tank and analysed for product distribution by either gas chromatography (Akiti, 2000) or HPLC (Baldyga et al., 2001). Test-reaction reported for low turbulence in the tank, with dissipation rate as low as 0.018 $W \cdot kg^{-1}$ (Baldyga et al., 1997).
Iron sulphate	Sodium hydroxide	Ethyl monochloroacetate	$k_1 = 10^7$; k_2 = 0.023	Baldyga and Bourne [43]	Titration. Limiting reagent B is added to a tank containing reagents A and C. The concentration of ferric ions still present in solution after reaction (not precipitated as ferric hydroxide) is found by titration with EDTA in the presence of salicylic acid at pH≈3
Benzene	NO^{2+} (as NO_2BF_4)	Toluene	k_1/k_2 = 27	Baldyga and Bourne [43], Tolgyesi [44]	Gas chromatography technique. B is added to an equimolar mixture of A and C in a stirred tank. After reaction is complete, samples are taken from the batch reactor and the distribution of products between nitrobenzene and nitrotoluene is measured by gas chromatography.

Benzoic acid	Sodium hydroxide	Ethyl chloro-acetate	$k_1 \rightarrow \infty$; $k_2 = 0.023$	Jasińska [8], Baldyga et al. [45]	Chromatographic analysis by one of two methodologies: (a) B is added to a mixture of A and C in a batch mixer. After reaction is complete, samples are taken and concentration of ester and/or by-product ethanol is measured by either GC or HPLC (Baldyga et al., 2012); (b) a solution of A and C in toluene is added to B in a batch mixer. After reaction is complete, concentrations of ethanol and ethyl chloroacetate are measured by Gas Chromatography (Baldyga et al., 2012; Jasińska, 2015).
Borate ion (boric acid)	Sulphuric acid	Iodide and iodate	$k_1 = 10^8$; $k_2 = f(I)$, I = ionic strength	Hecht et al. [36], Fournier et al. [46], Guichardon and Falk [47], Ghanem et al. [48]	$H_2BO_3^- + H^+ \leftrightarrow H_3BO_3$ $5I^- + IO_3^- + 6H^+ \leftrightarrow 3I_2 + 3H_2O$ $I_2 + I^- \leftrightarrow I_3^-$ Absorption Spectrophotometry technique. Iodate and iodide are added into a stirred tank. Sodium hydroxide is added before boric acid to prevent the formation of iodine in acid medium. When the reagents are supposed to be mixed, sulphuric acid is added into the stirred tank. The analysis of the solution is made by spectrophotometry at 353 nm within a minute after the end of reaction: samples taken two minutes after the acid injection – (Guichardon and Falk, 2000).
Sodium hydroxide	HCl	2,2 – dimethoxy-propane	$k_1 = 1.3\text{-}1.4 \times 10^8$; $k_2 = 0.6$	Bourne [31], Baldyga et al. [49]	Chromatographic analysis. HCl is added to a solution of alkali and acetal in a 1:10 ratio (v/v). According to Baldyga *et al.* (2012), equal molar quantities of acid and acetal should be used with a 5 % excess of alkali to ensure the stability of the unreacted acetal when all the acid has been neutralised. Mixing performed in a stirred tank, with analysis of product mixtures performed by gas chromatography.

Table 3. Operational parameters for several luminescence methods for assessing micromixing.

Reagent A	**Reagent B**	**Reagent C**	**Kinetic rate constant (25 °C)** [$m^3 \cdot mol^{-1} \cdot s^{-1}$]	**Reference**	**Analytical Method**
Ca^{2+} ions ($CaCl_2$)	Fluo-4 - reactive dye	Carboxy-SNARF - inert dye	$k = 10^6$	Faes and Glasmacher [50], Kling and Mewes [51], Wheat and Posner [52]	Fluo-4 + $CaCl_2$ → Fluo-4.Ca [with emission increase] LIF Technique. A mix of the two dyes is injected in the mixing vessel containing $CaCl_2$, which turns on the fluo-4 fluorescence; Excitation light source: Pulsed laser with λ=495 nm; Emitted light detected by a CCD camera at 516nm for Fluo-4 and 645 nm for Carboxy-SNARF.
Acid-base (HCl+NaOH)	Uranine (reactive dye)	Pyridine-2 (inert dye)	Quasi-instantaneous, $k \rightarrow \infty$	Lehwald et al. [2], Lehwald et al. [53], Lehwald et al. [54]	HCl + NaOH ↔ NaCl + H_2O @ pH=7 Uranine's emission E = *f*(pH) LIF Technique. Mixtures of water+acid+uranine+pyridine 2 (Flow 1) and water+base+uranine (Flow 2) flow to a mixer where they are illuminated at 532 nm; Emitted light detected by means of CCD cameras, at 550 nm for uranine and 705 nm for pyridine-2. Reported results refer to laminar regime.
Fe^{2+} ions – as $(NH_4)_2Fe(SO_4)_2$	Rhodamine – B, RhB	Hydrogen Peroxide, H_2O_2	$k_1 = 0.1$; $k_2 = 10^4 - 10^7$	Liu et al. [1], Hu et al. [14], Hu et al. [30]	$Fe^{2+} + H_2O_2 \leftrightarrow OH^{\bullet}$ $OH^{\bullet}$ + RhB → M [quenching of the fluorescence] LIF Technique. The fluorescent dye is dissolved in one of the reagent streams, so that when they mix, the reaction quenches the fluorescent signal; Light Source wavelength: 532 nm; Emitted light detected at 590 nm by means of CCD camera; Reported measurements performed online in mini-scale Y jet-mixers (Liu et al., 2009) or in unbaffled stirred tanks (Hu et al., 2012, 2010).
Water	Water + rhodamine B	NA	NA	Fall et al. [55]	LIF Technique. The fluorescent dye is dissolved in one of the two water flows that will be illuminated; Light Source wavelength: 520 nm. Emitted light detected at 590 nm by means of

					a CCD camera; Measurements reported performed online in a cylindrical stirred tank.
Cu (II) in NH_3 - NH_4^+ buffer (pH=11)	Luminol	Hydrogen Peroxide, H_2O_2		Rule and Seitz [56]	$C_8H_7O_3N_3 + Cu(II) + H_2O_2 \rightarrow$ 3-aminophtalate + $h\nu$ Chemiluminescence detection. The reagent flows are injected to the detection cell. No light source is needed; Emitted light detected by a photomultiplier tube at 420-450 nm; Measurements reported were performed online in a coil of Teflon tube that is pressed against the PMT detector; laminar regime
bis-(2,4,6-trichloro-phenyl)oxalate TCPO	Acriflavine	Hydrogen Peroxide, H_2O_2		Shamsipur et al. [57]	TCPO + $H_2O_2 \rightarrow C_2O_4 + 2\ [C_6HOCl_3]$ C_2O_4 + acriflavine $\rightarrow 2CO_2$ + acriflavine* $\rightarrow 2CO_2$ + acriflvine + $h\nu$ Chemiluminescence detection; Reagents are mixed in a stirred glass mixer; No light source needed; Emitted light detected online by means of a photocell at 510-540 nm.
bis-(2,4,6-trichloro-phenyl)oxalate TCPO	3-aminofluoranthene (3-AFA)	Hydrogen Peroxide, H_2O_2 + base catalyst		Jonsson and Irgum [58]	TCPO + $H_2O_2 \rightarrow C_2O_4 + 2\ [C_6HOCl_3]$ C_2O_4 + 3-AFA $\rightarrow 2CO_2$ + 3-AFA* $\rightarrow 2CO_2$ + 3-AFA + $h\nu$ Chemiluminescence detection; No light source needed; Emitted light detected by a photomultiplier tube at 518 nm; Measurements reported were performed online in a stopped-flow equipment

2. Experimental Section

Test-Reactions

For AB-RPLIF method, the hypothesis of a reaction between a strong acid and strong base was first considered. The first preliminary test was conducted for a reaction between hydrochloric acid, HCl, and sodium hydroxide, NaOH [2, 53, 54]. The extreme sensibility of pH to the smallest variation in the acid and base concentrations hinders the results' reproducibility.

So, the AB-RPLIF method was implemented for a reaction between phosphoric acid, which is a polyprotic acid, and NaOH. The titration curve of a weak acid and a strong base is smoother than the strong acid – strong base curve. This fact enables to easily detect the increase in pH and the respective change in fluorescence emission. The acid-base test-reaction system used is

$$H_3PO_4 + NaOH \leftrightarrow NaH_2PO_4 + H_2O \quad (1a)$$

$$NaH_2PO_4 + NaOH \leftrightarrow Na_2HPO_4 + H_2O \quad (1b)$$

$$\underline{Na_2HPO_4 + NaOH \leftrightarrow Na_3PO_4 + H_2O} \quad (1c)$$

$$H_3PO_4 + 3NaOH \leftrightarrow Na_3PO_4 + 3H_2O \quad (1d)$$

As most of acid-base reactions, the reaction scheme in Equations (1a, 1b, 1c) is quasi-instantaneous, and thus the kinetic rate constant is $k \to \infty$. This is necessary for visualization of the micromixing regions without delay that would shift the location of micromixing and the appearance of the tracer.

Fluorescein is the tracer used in this test-reaction (Equation (1d)). When fluorescein is excited by a laser, the emission intensity of fluorescein depends on the local pH. When an acid stream, containing fluorescein, is mixed with a base stream, the local pH modification and respective changes on the emission intensity of mixture can be used for monitoring the neutralisation reaction kinetics. The variations in the emission intensity enable the visualisation of micromixing dynamics in the reaction system.

The second test-reaction studied in this work uses Fenton's reaction to quench the fluorescence signal, so that the reactive mixing process can be recorded quantitatively (Liu et al., 2009). Fenton's reaction is a redox reaction which is induced by the coupling of iron, Fe^{2+}, and hydrogen peroxide, H_2O_2,

$$Fe^{2+} + H_2O_2 \rightarrow Fe^{3+} + HO\bullet + OH^- \quad (2a)$$

$$HO\bullet + RhB \rightarrow RhB_{oxi} \quad (2b)$$

In this approach, the fluorescence tracer RhB is dissolved in one or both streams to be mixed, being oxidised with the hydroxyl radical (HO•) (Equation (2b)). The vanishing of RhB enables the reaction kinetics based on the relationship between emission and fluorophore concentration.

Experimental Procedure – Study of the test-reactions

In the acid-base reaction, the concentration of H_3PO_4 (Fisher, > 97 % purity) was determined according to the best balance between operational costs and the pH values for fluorescence detection. Based on that, the H_3PO_4 concentration of 0.100 M was prepared, and the concentration of NaOH (Fisher, 99.3 % purity) was defined from the H_3PO_4:NaOH titration curve, [NaOH]=0.165 M, for $pH = 7$.

For Fenton's reaction, different concentrations of H_2O_2 (Fisher, > 97 % purity) and Fe ($FeSO_4 \cdot 7H_2O$, Fisher, > 97 % purity) were tested according to the vanishing rate of RhB. For higher concentrations of Fe and H_2O_2, the oxidation rate is higher, and simultaneously it is observed the formation of iron sludge as the results of the conversion of Fe^{2+} to Fe^{3+}. For lower concentrations, the reaction course is slower, and there is a decrease in the

production of iron sludge. From those results, the concentrations used were 2 % H_2O_2 (wt./v) and 0.010 M Fe^{2+}.

The suitable operating conditions to quantify mixing from these two test-reactions were tested in an SX.18MV Reaction Analyzer Stopped-Flow (SF) apparatus from Applied Photophysics. An ozone-free xenon lamp (cut off at 250 nm) was used as a light source. The excitation wavelength was controlled by a monochromator, connected to the sample handling unit optical cell through a light guide. The sample handling unit consisted of two drive syringes whose plungers are moved by a pneumatic ram. Downstream of the driving syringes, the reagents are set in contact in the 10 μL mixing chamber and flow down through a 20 μL optical cell, which consisted of a silica square tube of 10 mm length. A photomultiplier tube (PMT) is installed in a normal position to the optical cell (optical pathlength is 2 mm) to detect the absorbance or the emission intensity, according to the chosen operating mode. PMT converts the light into an electrical signal to determine the absorbance or the fluorescence (emission intensity).

The absorption spectra of fluorescein (Panreac, 99 % purity) and RhB (Acros, 98 % purity) were determined from PMT in a wavelength range from 250 to 700 nm. However, the layout of the equipment did not enable the assessment of tracers' emission wavelength, so the emission peak was not estimated in this work. The excitation peak was predicted from the absorption spectrum, and then this value was compared to the one in the literature. The comparison of both values validates the method.

The set of experimental conditions was designed aiming to assess the conditions under which these reactions could be efficiently used as test-reactions for mixing studies. The experimental conditions are summarised in Table 4.

Solutions with different concentrations of RhB and fluorescein were prepared, and the absorption spectrum (from 250 to 700 nm) was determined in SF for each concentration (essays F1 and RhB1 in Table 3). The excitation peak was determined from the absorption spectrum.

Karasso and Mungal [59] tested the relationship between the emission intensity and the concentration of fluorescein for an excitation wavelength of 532 nm. The limit of linearity concentration is 10 $mg \cdot L^{-1}$ for fluorescein. However, Karasso and Mungal [59] reported that the fluorescence intensities at this concentration range are too low for imaging. Therefore, the response of fluorescein was tested for higher concentrations in F2 (Table 3).

Concentration range was defined based on the operation restrictions of the measurement equipment: high enough to minimize equipment noise, but within the maximum limit of detection. Linearity range was also considered while defining the studied range. Regarding pH (in AB-RPLIF), essays F1 and F2 were performed aiming at $pH = 7$ upon mixing/reaction to ensure the highest emission intensity by fluorescein (see Fig. 4). It also corresponds to a smoother zone of the H_3PO_4 + NaOH titration curve, which minimizes variation in the observations due merely to the dosing of chemicals to the mixing chamber. Essay F3 was performed in a wide pH range to explore the effect of this parameter on fluorescein's emission intensity. Essay F4 was performed at $pH = 2$, since fluorescein was to be supplied with the acid (H_3PO_4) stream, to ensure minimal emission at those conditions.

Table 4. Experimental conditions of AB-RPLIF and Oxi-RPLIF methods.

Essay	Objective	C [mg·L^{-1}]	pH	Time of measurements
F1	Absorption Spectrum	4; 20	7	Immediately after preparation
F2	Linearity dynamic range of fluorescence	4 - 30	7	Immediately after preparation
F3	pH effect on emission	20	2-12	Immediately after preparation
F4	Fluorophore stability	20	2	Immediately after preparation and 24 h after preparation
RhB1	Absorption Spectrum	0.5		Immediately after preparation
RhB2	Fluorophore stability	0.5		Immediately after preparation and 24 h after preparation

For RhB, the linearity range for an excitation wavelength of 532 nm has already been reported by Mortensen et al. [60]. Thus, the dependence between the concentration of RhB and its fluorescence was not determined experimentally.

The readings were repeated after 24 hours to assess the impact of ageing on the spectra, which could limit the usability of the method within that period. This period represents the preparation of the reagents from one workday to the following (essays F4 and RhB2 – Table 3).

For the acid-base reaction, an additional parameter was studied, which is the relationship between pH and fluorescence. Fluorescein solutions were prepared at different pH, and the emission spectra were determined (essay F3 – Table 3).

Experimental Procedure – Validation of test-reaction in a T-jets mixer

The RPLIF methods were tested in a T-Jets reactor, which consists of two opposite feeding channels connected to a mixing chamber making up an angle of 90º. A schematic drawing of the T-Jets geometry used in this work is shown in Figure 1.

When two liquid streams are fed through the opposed jets, the reaction occurs in the mixing chamber promoted by the mixing of the two streams. The mixture leaves the mixing chamber through an open outlet. The characteristic dimensions of T-Jets are also illustrated in Figure 1: the width of the mixing chamber, W, the width of injectors, w, and the depth of the mixing chamber, d.

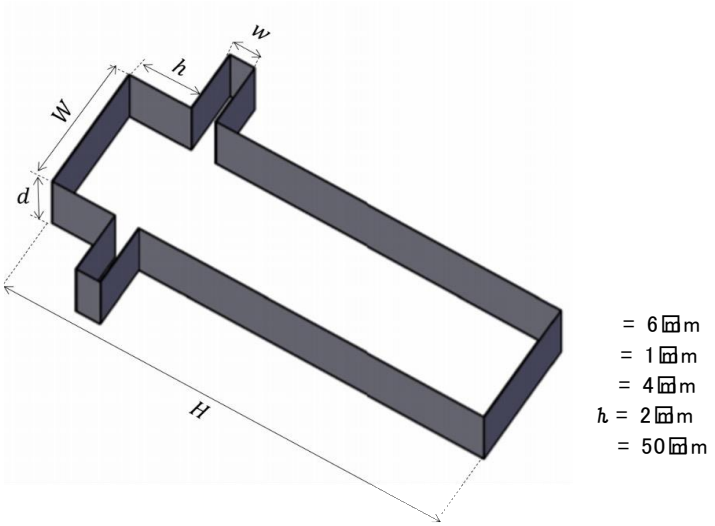

Figure 1. Sketch of T-Jets geometry.

Many studies on T-Jets show that the mixing and flow dynamics in the mixing chamber depend on the operating conditions, which are mostly associated to the Reynolds number. However, Sultan et al. [61] reported from PLIF images and Computational Fluid Dynamics (CFD) simulations that the geometric parameters also affect the flow dynamics. Thus, the flow regime in T-Jets depends on the momentum ratio of the jets, the chamber-to-injector width or chamber width-to-depth ratios and the jet's Reynolds number, which is defined (Sultan et al., 2012)

$$\mathrm{Re} = \frac{\rho v_{\mathrm{inj}} W}{\mu} \tag{3}$$

where ρ and μ are the density and the viscosity, respectively, and v_{inj} is the injector fluid velocity.

Different combinations of operational and geometrical parameters result in four flow regimes in T-Jets:

- Segregated or stratified flow regime – a steady flow regime where each side of the mixing chamber contains mainly one of the fluids. The fluid stream flows from the jets to the outlet delimited by the segregation plane that coincides with the mixing chamber axis and is normal to the inlet's axes (Bothe et al., 2008; Soleymani et al., 2008a; Sultan et al., 2012);
- Vortex flow regime – steady flow regime which is characterised by the formation of Dean vortices in each side of the mixing chamber. These vortices are characterised by a helicoidal movement inside of each liquid stream, and their rotation axis is aligned with the mixing chamber axis (Bothe et al., 2008; Mariotti et al., 2018; Soleymani et al., 2008a, 2008b; Sultan et al., 2012);
- Engulfment flow regime – the symmetry is broken, and the fluid streams injected by each injector rotate over the chamber axis creating a single vortex that engulfs both streams. This promotes the transport of fluid from one half of the chamber to the other (Bothe et al., 2008; Soleymani et al., 2008a; Sultan et al., 2012; Zhang et al., 2019);
- Chaotic flow regime – this flow regime is characterised by the formation of a vortex street, resembling a von Karman vortex street, consisting in the shedding of vortices from the opposed jets impingement point which evolves throughout the mixing chamber promoting the fast mixing of the fluid streams (Sultan et al., 2012).

Sultan et al. (2013, 2012) defined the transition regime as the onset of chaotic flow regime, which is characterised by the formation of mixing structures, i.e., vortex streets.

The critical working conditions for the onset of self-sustainable chaotic flow regimes are $W/w = 6,\ W/d \geq 2$ and Re above 300.

The implementation of reactive PLIF (RPLIF) methods was conducted in a T-Jets reactor with a typical geometry shown in Figure 1. In this work, only one geometry was tested with a height of $H = 50$ mm, a mixing chamber width of 6 mm, a width of injectors of 1 mm and a depth of 4 mm (W6w1d4). The selection of this geometry was based on the previous studies, where it is observed that this is the best combination for the onset of the self-sustainable flow regime [61].

In AB-RPLIF method, the acid stream, phosphoric acid (H_3PO_4) and fluorescein, was stored in one of the tanks and the base stream, sodium hydroxide (NaOH), was stored in the other one. Three different flow regimes were tested: $\mathrm{Re} = 50$, $\mathrm{Re} = 150$ and $\mathrm{Re} = 200$ where Re is defined from the width of injectors (Equation (3)). The operating conditions were symmetric, i.e., the acid and base liquid streams have the same viscosity, density and flow rate, i.e., $\mathrm{Re_{acid}} = \mathrm{Re_{base}}$. Experiments were conducted injecting the acid fluid stream through the left-side injector and the base fluid stream through the right-side injector.

In Oxi-RPLIF method, the iron (Fe^{2+}, as $FeSO_4$) was stored in one of the tanks and the hydroxide peroxide (H_2O_2) was stored in the other one. Both streams were doped with rhodamine B (RhB). Oxi-RPLIF was tested in T-Jets mixers for two different flow regimes: $\mathrm{Re} = 50$ and $\mathrm{Re} = 150$. The operation conditions are symmetric, i.e., solutions delivered from both injectors have the same viscosity, density and flow rate, i.e., equal Reynolds number, $\mathrm{Re_{iron}} = \mathrm{Re_{H_2O_2}}$.

The RPLIF methods require the use of a laser sheet that will illuminate the plane within the flow of the acid stream doped with fluorescein (in AB-RPLIF) or the hydrogen peroxide and iron dyed with RhB (in Oxi-RPLIF). Fluorescein and RhB will emit fluorescence enabling the visualisation of the reactive regions.

3. Results

AB-RPLIF Method

The absorption spectrum relates the excitation wavelength and the absorbance of the molecules of the fluorescent tracer. Figure 2 shows the absorption spectra of fluorescein for an excitation wavelength from 200 to 700 nm for two distinct concentrations 4 mg·L^{-1} and 20 mg·L^{-1}. The excitation peak of this dye is near 490 nm for both concentrations, which is in agreement with the value in the literature [62]. On the other hand, the literature points to an emission peak of 514 nm, and a red tail that continues to 640 nm [62].

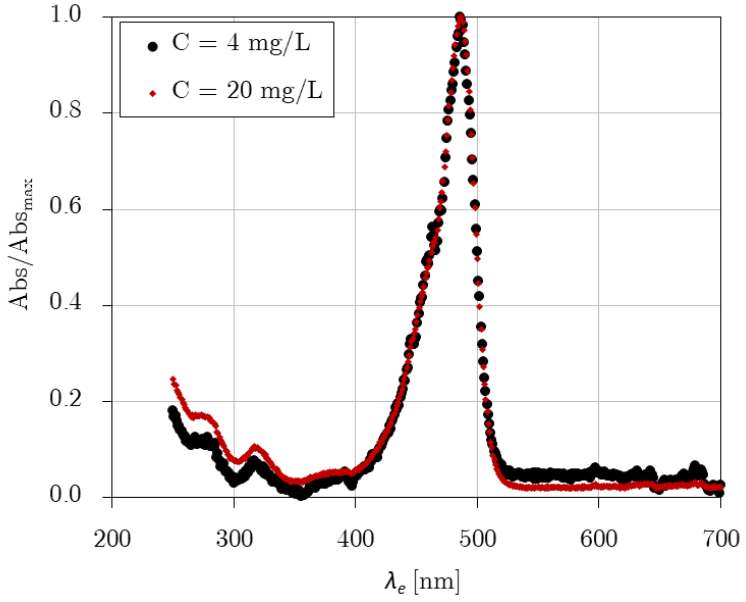

Figure 2. Absorption Spectra of fluorescein for an excitation wavelength from 200 to 700 nm for 4 mg·L^{-1} and 20 mg·L^{-1} in H_3PO_4 0.100 M + NaOH 0.165 M medium, pH = 7.

The successful implementation of this technique in flow phenomena studies requires the selection of suitable working conditions. The laser should have an emission peak near the excitation peak of fluorescein, which is approximately 490 nm.

Fluorescein is frequently combined with an Ar-ion laser for quantitative LIF imaging experiments in flow phenomena studies [63, 64]. The efficient excitation of fluorescein molecules occurs at 488 nm line of an argon-ion laser. Calibration curves showed that there is a linear relationship between the fluorescence and the dye concentration, which is the desired behaviour. This result is in agreement with the Beer-Lambert law, which relates the absorbance and the properties of the absorbing species, such as the concentration of species.

Karasso and Mungal [59] tested the combination of fluorescein with a pulsed Nd:YAG laser. Nd:YAG lasers enable a significant temporal resolution and are easily implemented and widespread in performing 2D images. Nd:YAG laser used by Karasso and Mungal [59] and in most PIF/PLIF setups operate at 532 nm. The absorption spectrum of fluorescein (Figure 2) shows a deficient value for an excitation wavelength of 532 nm. Karasso and Mungal [59] test the linearity between the fluorescence and the dye concentration for Nd:YAG laser. The results reported a linear region up to 10 mg·L^{-1}. Then, higher concentrations of fluorescein were tested to achieve the same signal level obtained with an Ar-ion laser. Results showed that the signal calibrations violate the Beer-Lambert law and a non-linearity of fluorescence versus local excitation intensity is detected likewise. Therefore, the combination of fluorescein and Nd-YAG laser will bring problems in the image post-processing and the respective quantification from the relationship between the concentration and fluorescence. However, this combination could naturally be used for any qualitative imaging or flow visualisation.

Since Nd:YAG laser is widely used in experimental fluid mechanics setups, further studies on emission intensity for higher concentrations of fluorescein are addressed in this work. The fluorescence of fluorescein was measured for a concentration range between 4 and 30 mg·L^{-1}. Figure 3 shows the electric potential difference detected versus the concentration of fluorescein at four excitation wavelengths, Figure 3a for 350, 488, 500 and Figure 3b for 532 nm. The data were split into two plots because for 532 nm the values are orders of magnitude below the ones obtained for other wavelengths.

The emission intensity displays a linear trend ($R^2 > 0.97$) with fluorescein concentration up to at least 30 mg·L^{-1} for all tested excitation wavelengths, as shown in Figure 3. The large values of emission intensity are detected at $\lambda_e = 488$ nm, which corresponds to the peak in absorption spectra (Figure 2). For $\lambda_e = 532$ nm, the electric potential is low, and so weak fluorescence will be emitted in a range up to 30 mg L^{-1}. Despite this quantitative analysis, the of fluorescein with Nd-YAG Laser is only demonstrated for qualitative imaging of micromixing.

The influence of pH on emission intensity of fluorescein is also determined adding NaOH solution to H_3PO_4. Figure 4 shows the electric potential difference detected for fluorescein versus pH at four excitation wavelengths, 350, 488, 500 in Figure 4a and 532 nm in Figure 4b. Likewise in Figure 3, the wavelengths for 350, 488 and 500 nm are in a separate plot than those for 532 nm due to the large difference in values between data series. As observed from the variations of electric potential, the fluorescein emits for pH above 3 and reaches its maximum emission at pH $\cong$ 8. For pH between 5 and 8, the curve sharply increases, and so the maximum sensitivity of emission depends on local pH and the reaction course. These results corroborate the findings of Kola and Amataj [65] and Lehwald et al. [2]. The curves displayed in Figure 4 overlaps the pH range where the H_3PO_4:NaOH titration curve is smooth, enabling the detection of small differences of mixing degree at local scale.

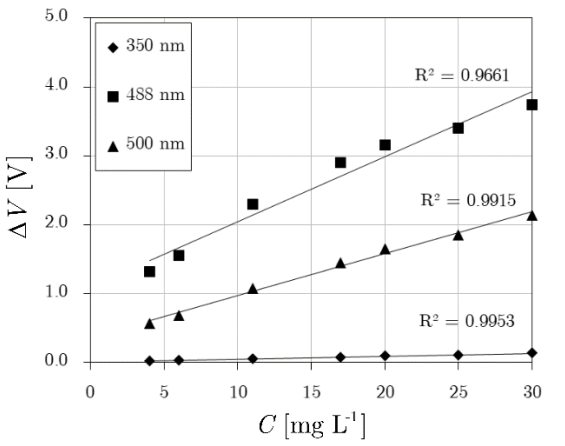

(a)

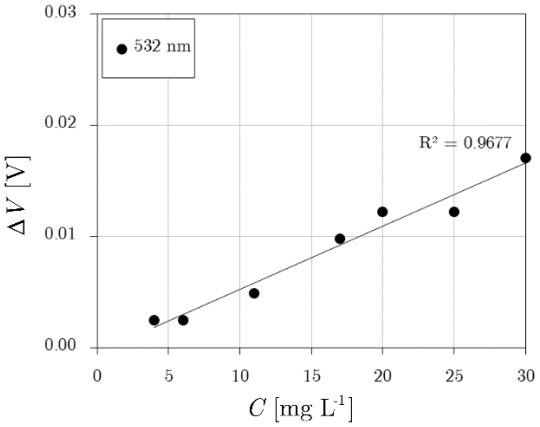

(b)

Figure 3. Electric potential difference for fluorescein for different concentrations at different excitation light wavelengths in H_3PO_4 0.100 M + NaOH 0.165 M medium, pH = 7 for a) 350 to 500 nm, and b) 532 nm.

These results showed that qualitative measurements of mixing employing this test-reaction could be conducted for concentrations of fluorescein up to 30 mg·L^{-1} with Nd:YAG laser, under excitation wavelengths in a range from 475 to 532 nm.

Figure 5 shows the electrical potential difference versus the excitation wavelength for fresh fluorescein and the repetition of this test one day later. Ageing of reagents did not have an impact on the intensity emission in any way that would prevent the use of this test-reaction within a 24 h period. This is another encouraging feature of this method.

The implementation of this reaction scheme coupled to the imaging of fluorescence emission in a plane illuminated by a laser shows the reactive fronts in a flow. This method would enable to show the structure of interfacial area generation between two reactants being mixed.

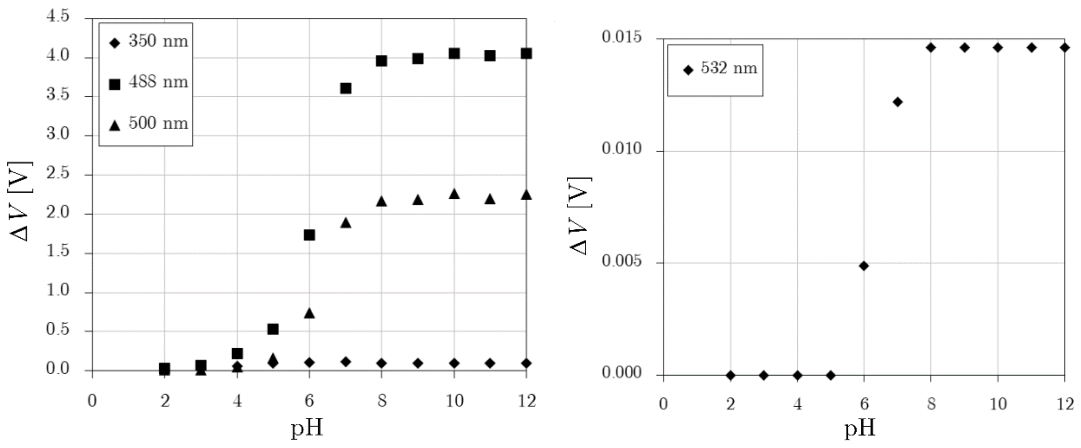

Figure 4. Influence of pH on electric potential difference measured for 20 mg·L^{-1} fluorescein solution at 25 ºC, for a) 350 to 500 nm, and b) 532 nm.

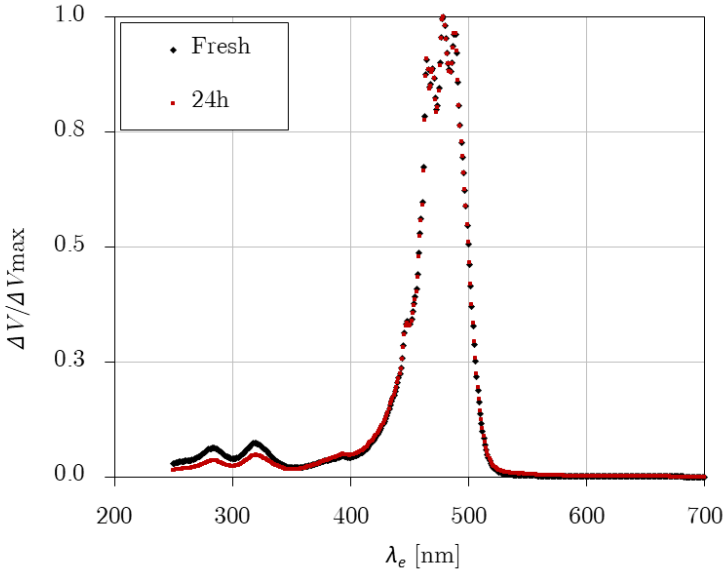

Figure 5. Electric potential difference associated to fluorescein versus the excitation wavelength for 20 mg·L^{-1} solution in H_3PO_4 0.100 M + NaOH 0.165 M medium, immediately after preparation and 24 h later.

A narrow-band filter is usually placed in front of the camera lens to only capture the fluorescence wavelengths in the performance of AB-RPLIF method in T-Jets mixers. As the emission peak of fluorescein is approximately 510 nm, the narrow-band filter used in this method may filter the wavelengths in a range > 500 nm empowering the capture of the emission wavelengths of fluorescein and filtering the light of laser.

Figure 6 shows RPLIF images obtained at the plane defined by the mixing chamber and injector axis, for AB-RPLIF method at $\mathrm{Re_{acid}} = \mathrm{Re_{base}} = 50$. At the inlet, the acid fluid stream has $pH \cong 2$, and thus the emission intensity of fluorescein was approximately 0, as observed from Figure 4. Therefore, the fluid issuing from this jet is capture as dark in PLIF images. These PLIF images show that the fluorescein concentration is enough for imaging, even for $\lambda_e = 532$ nm.

PLIF images in Figure 6 show that no dynamic structures are formed in the mixing chamber, and thus each fluid stream remains in each side of the mixing chamber. Figure 6 also shows the appearance of white flow patterns in the mixing chamber which results from increasing the pH of the acid stream that is associated with an increase of the

emission intensity of fluorescein. These visualisations show that the acid-base reaction of H_3PO_4 and NaOH occurs in the T-Jets mixing chamber, and the flow regime is commonly named by the vortex flow regime (Santos and Sultan, 2013).

These results are in agreement with Bothe et al. [66] and Hoffmann et al. [67], who reported that, at this flow regime, there is the transport of one fluid from one side to the other due to convective mechanisms. Although these convective mechanisms are not visualised from non-reactive PLIF methods, the appearance of a white colour fluid in AB-RPLIF method enables to conclude that the convective mixing phenomena promote the reaction of H_3PO_4 and NaOH. These convective mechanisms consist of two parallel Dean vortices, particularly visible from the pathlines of segregated regime, which is generally referred in T-jets literature as vortex flow regime, reported Soleymani et al. [68], Soleymani et al. [69].

In Figure 6, it is also observed the formation of a vortex in each side of the mixing chamber head. Sultan et al. [61] had already reported the formation of two upper vortices from the intrusion of fluid having different colour in one of the jet streams. These two upper vortices are symmetric and roundish. The residence time in these vortices is generally large, compared with the flow passage time in the mixing chamber, and so there is local accumulation of reaction product in this region.

Once again, the conclusions on the classification of the flow regime could be clear from the observations of the cross-section of the mixing chamber made from the top of T-jets mixer. It would be expected to visualise a double pair of counter-rotating vortical structures.

Figure 7 shows AB-RPLIF images obtained at the plane defined by the mixing chamber and injector axis at $\mathrm{Re}_{\mathrm{acid}} = \mathrm{Re}_{\mathrm{base}} = 125$. The flow is no longer at steady state (segregated or vortex flow). The opposite jets are impinged at the mixing chamber axis and directed towards the outlet, with the formation of vortices on both sides of the jets. These vortices evolve throughout the mixing chamber towards the outlet: vortex street. The mixing of two streams promotes the acid-base reaction and thus, the pH increases throughout the mixing chamber. This results in the increase of the intensity of emission of fluorescein and the appearance of white colour.

The acid-base reaction is practically instantaneous, and thus the reaction time is very small. This means that there is a general spread of tracer in the reactor, showing product reaction at the contact region of the two streams, which now extends throughout the mixing chamber.

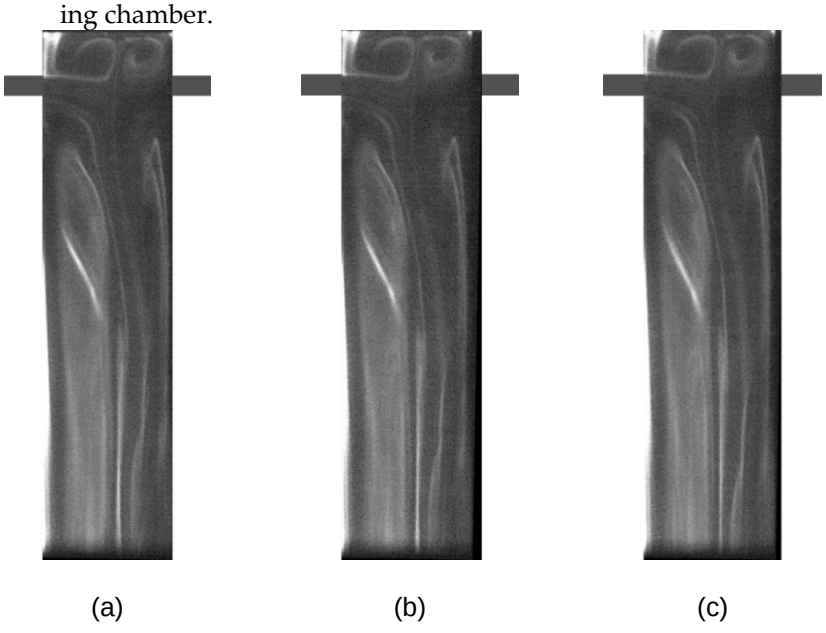

Figure 6. PLIF image obtained from AB-RPLIF method at $\mathrm{Re} = 50$.

Figure 8 shows a sequence of AB-RPLIF images obtained at $Re_{acid} = Re_{base} = 200$. The overall formation of vortices promotes the interfacial area generation between the two inlet streams resulting in the same observations at $Re = 125$ in Figure 7.

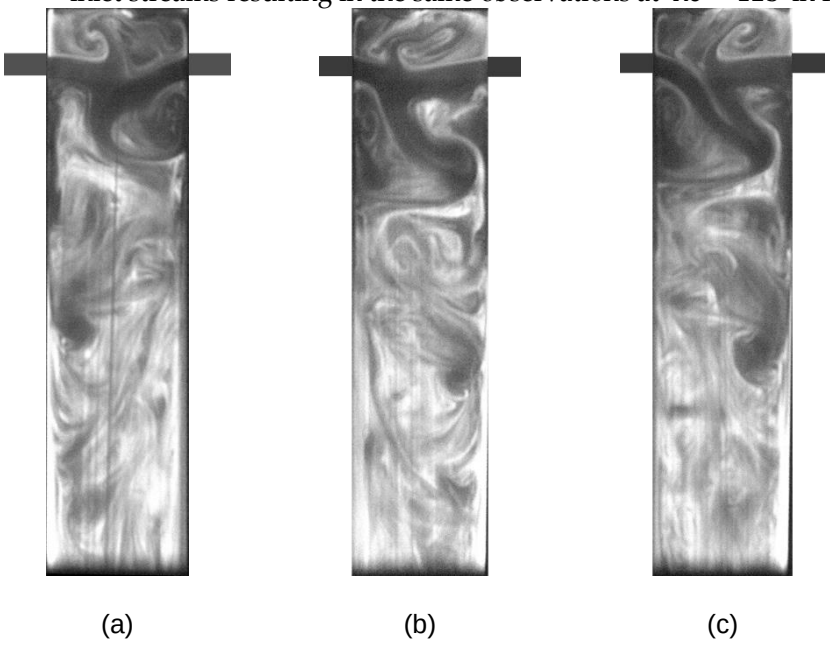

Figure 7. PLIF image obtained from AB-RPLIF method for $Re = 125$.

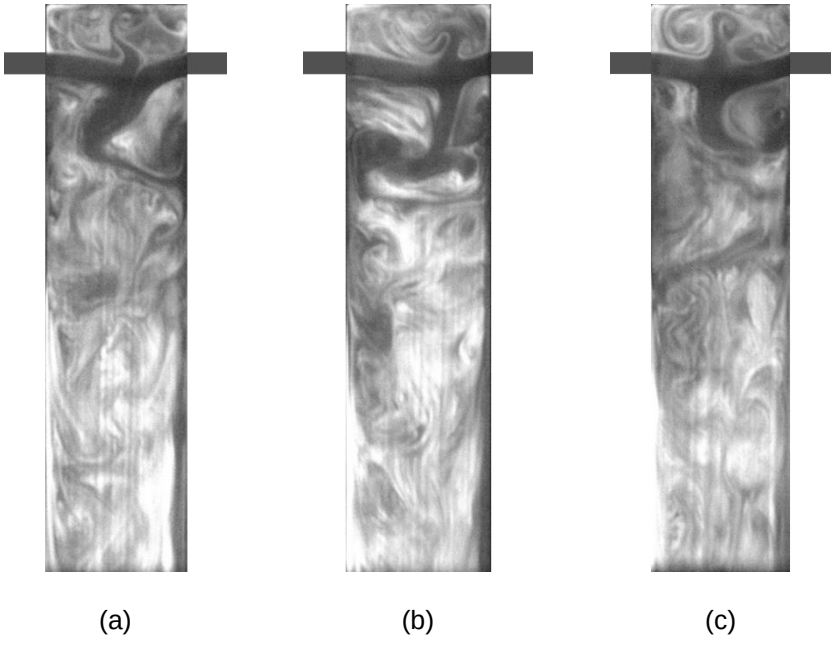

Figure 8. PLIF image obtained from AB-RPLIF at $Re = 200$.

The experimental conditions ($Re = 50$, $Re = 100$ and $Re = 200$) tested using RPLIF were also simulated in Sultan et al. [70] and Sultan et al. [71]. Simulation results also show that the self-sustainable chaotic mixing is onset for $Re > 125$, as observed in Figure 7.

The combination of AB-RPLIF and Nd:YAG laser does not permit the quantification of mixing from post-processing of PLIF images, because it is not possible to work at a linear concentration region with this laser.

Nevertheless, AB-RPLIF method enabled the visualisation of the reactive regions in T-Jets mixers at chaotic flow regimes for the first time. The regions where the reaction

already took place are marked by a high emission intensity enabling to identify the reactive regions.

Oxi-RPLIF Method

RhB was used as a fluorescent tracer for Fenton's reaction. The absorption spectrum shows the relation between the excitation wavelength and the absorbance of RhB molecules. Figure 9 shows the absorption spectrum of RhB for an excitation wavelength from 200 to 700 nm for a concentration of 0.5 mg·L^{-1} at 20 ºC. The excitation peak of this dye is near 550 nm for both concentrations, which is in agreement with the value in the literature [62]. According to Crimaldi [72], the absorption spectrum is broad enough to be excited in a range from 514.5 to 532 nm.

Coppeta and Rogers [62] detected the emission spectrum of RhB and the respective emission peak, which occurs at 580 nm.

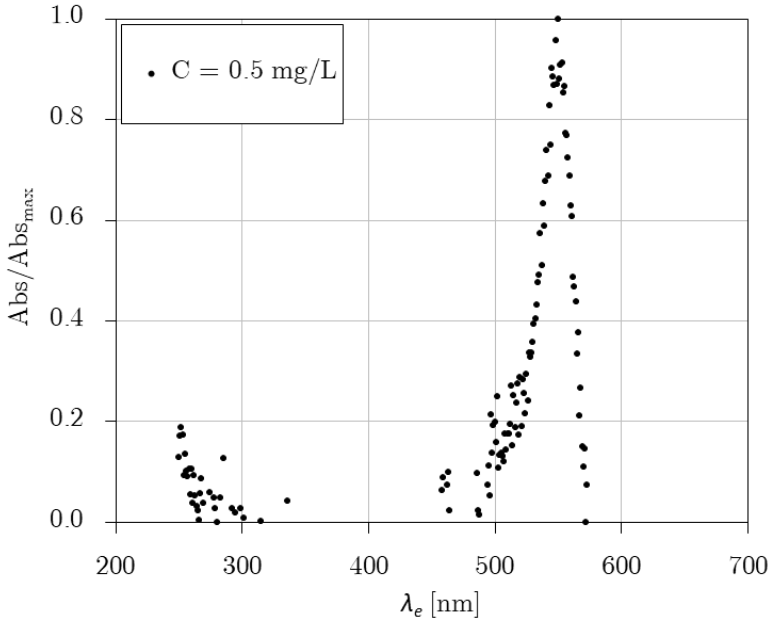

Figure 9. Absorption spectra of RhB for an excitation wavelength from 200 to 700 nm for 0.5 mg·L^{-1} at 20 ºC.

The absorption spectrum shows that RhB molecules absorb strongly at 532 nm and thus Nd:YAG laser is suitable to this method. Mortensen et al. [60] determined the calibration curve for RhB concentration and fluorescence intensity using Nd:YAG laser. Results identify a linear region for the local fluorescence and the local emission intensity up to 0.6 mg·L^{-1}. As expected, the local fluorescence decreases with the concentration of RhB, so the oxidation of RhB during the reaction course promotes the absence of fluorescence. The implementation of Fenton's reaction permits the flow visualisation and the identification of reaction regions, which are detected from the vanishing of the RhB fluorescence. The linearity between the RhB concentration and the fluorescence observed with Nd:YAG laser makes this method suitable for quantitative imaging.

When a pulsed Nd:YAG laser is combined with RhB and Fenton's reactions, a narrow-band filter should be placed in front of the camera lens to only capture the wavelength emitted by RhB. As mentioned in the literature, the emission peak of RhB is 580 nm, so the narrow-band filter used in this method may filter the wavelengths in a range > 540 nm empowering the capture of the emission wavelengths of RhB and filtering the light of the laser.

Considering 2 % H_2O_2 (wt./v) and 0.010 M Fe^{2+} concentrations (less than half the concentrations reported in the cited works), and using RhB in both streams, the ageing of reagents did not cause changes in the emission spectrum that would prevent the handling

of this test-reaction within a 24 h period. The non-ageing for 24 h is an encouraging feature of this method.

In the implementation of this method for the assessment of micromixing, the temperature should be controlled since the fluorescence of RhB is very sensitive to temperature [18].

This method converts Fe^{2+} to Fe^{3+} during the Fenton's reaction course, which results in the production of an iron sludge that may settle and could cause negative impacts on the mixing equipment used. Furthermore, in Fenton's reaction, there is the formation of oxygen that results of the dissociation of H_2O_2 into oxygen and water,

$$2H_2O_2 \rightarrow 2H_2O + O_2 \quad (4)$$

The generation of oxygen in the reaction course leads to the presence of bubbles in the flow, making it difficult to visualize in a closed geometry from where gas can get stuck. For stirred tanks the formation of small gas bubbles should not be a problem.

Experiments were conducted at 23 ºC. Figure 10 shows Oxi-RPLIF images obtained at the plane defined by the mixing chamber and injector axis at $Re_{iron} = Re_{H_2O_2} = 50$. The two liquid streams injected in the mixing chamber are white because both were dyed with RhB, which emits fluorescence when illuminated by a laser light sheet. Oxi-RPLIF images show that no dynamic structures are formed in the defined plane at that Re. The disappearance of tracer, associated to changes of liquid streams' colours, from white to black, is shown in Figure 10. This is related to the RhB oxidation by hydroxyl radical (HO•) (Equation (2b)).

Figure 10 also shows a darker central region on the contact of both reactant streams, where the reaction takes place. This is associated to two Dean vortices formed in each side of the mixing chamber (vortex flow regime) which promotes the reaction between Fe^{2+} and H_2O_2. These results are in agreement with Bothe et al. [66] and Hoffmann et al. [67] and even with the AB-RPLIF images shown in Figure 6.

Figure 11 shows Oxi-RPLIF images of the plane defined by the mixing chamber and injectors axis at $Re_{iron} = Re_{H_2O_2} = 150$. At these working conditions, the flow is no longer steady and stratified. Dynamic mixing structures are formed, promoting the engulfment of the two liquid streams. So, at these flow conditions, the disappearance of tracer is more generalised at downstream positions of the mixing chamber. And so, the use of Fenton's reaction as RPLIF method enables to assess chemical reaction rate throughout the reactor. The main mechanism in this method is the saturation of the inlet streams with a tracer and the respective disappearance of the tracer, which can be used as an indicator of the chemical reaction.

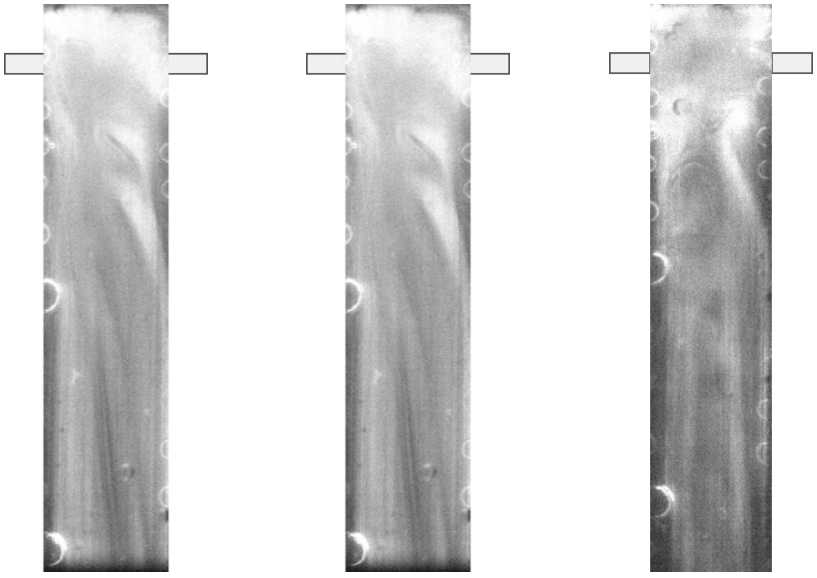

(a) (b) (c)

Figure 10. PLIF image from Oxi-RPLIF method at $Re = 50$.

Figure 10 and Figure 11 show the formation of gas bubbles during the experiments, that makes the visualisation of mixing even more difficult. The release of oxygen in Fenton's reaction, described by Equation (4), does not enable to quantify the mixing degree, such as from the intensity of segregation.

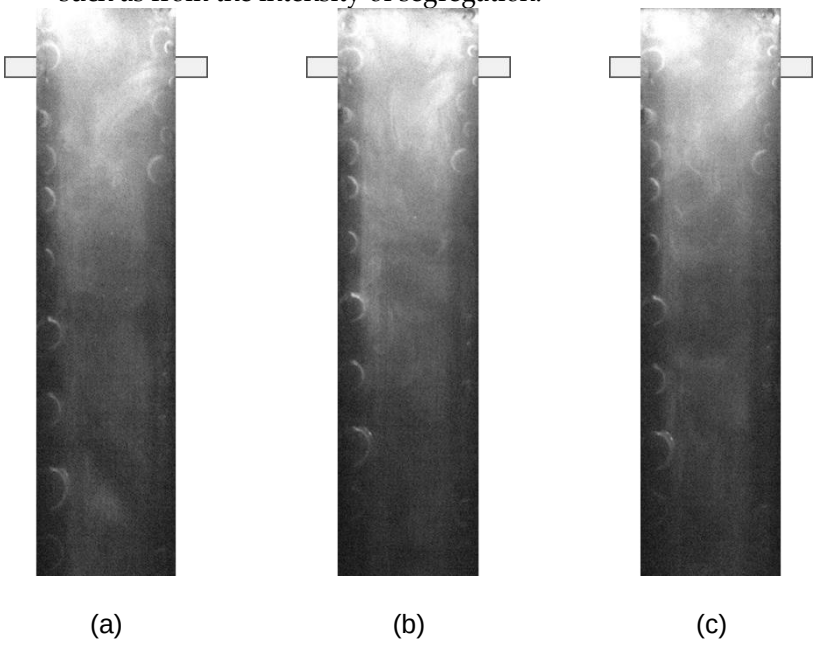

Figure 11. PLIF image obtained from Oxi-RPLIF method at $Re = 150$.

Figure 12 shows three RPLIF images using three different systems. In Figure 12a, one liquid stream was dyed with Rhodamine and the micromixing was assessed from the field of emission intensity of rhodamine, which is associated to its concentration. Figures 12b and 12c enable the flow characterization from reactive tracer in two test-reaction systems, AB-RPLIF and Oxi-PLIF. These images show that the mixing and flow regimes are more clearly observed from AB-RPLIF using fluorescein.

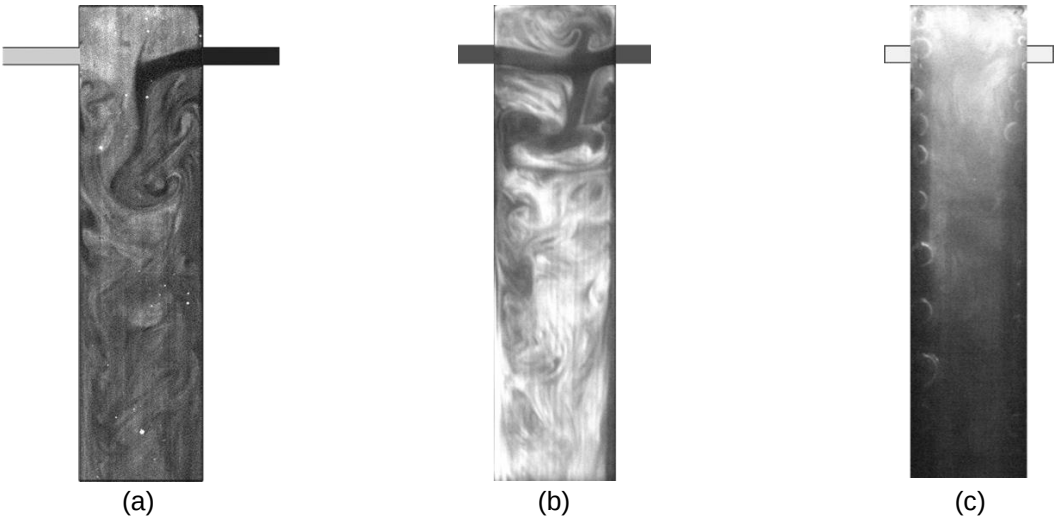

Figure 12. PLIF images obtained from (a) non-reactive Rhodamine tracer; (b) AB-RPLIF method; (c) Oxi-RPLIF method.

4. Economic analysis of AB-RPLIF versus Oxi-RPLIF method

The two RPLIF methods studied have associated costs that must be considered in the decision making process. In this work, operating costs were determined based on lab-scale average market prices of each chemical used, considering 1 m^3 of fluid flowing through the mixing chamber, and knowing that half of that volume is attributed to each stream.

Therefore, in AB-RPLIF method, in which the acid stream comprises 0.100 M H_3PO_4 and a maximum of 20 $mg_{fluorescein}·L^{-1}$, and the base streams consists of 0.165 M NaOH (for pH = 7), the operating cost of this method would be around 78 €·m^{-3}. The neutralisation inside the mixing chamber decreases the risk of accidents, which makes this method more promising. For Oxi-RPLIF method, the implementation cost at the studied conditions (2 % H_2O_2 (wt./v) and 0.010 M Fe^{2+} concentrations, with $mg_{RhB}·L^{-1}$ in both streams) would be 405 €·m^{-3}.

This cost estimative considers the use of analytical grade chemicals, which are associated to higher purchase costs than industrial grade reagents, which would also serve the purpose of visualization. Reagents at industrial quantities and grades, particularly H_2O_2, will enable to reduce costs by 90%.

5. Conclusions

Two test-reactions, acid-base reactive PLIF (AB-RPLIF) and Fenton's reaction (Oxi-RPLIF), suitable for mixing assessment/quantification, were studied and compared in this work. After adapting some of the operating conditions originally suggested in the literature, the test-reactions became easier and suitable to be used in micromixing studies. Suitable conditions to adopt employing AB-RPLIF would be 20 $mg_{uranine}·L^{-1}$ concentration in the acid stream; acid and base concentration in the streams enabling pH = 7 after reaction in the mixing chamber, such as 0.100 M H_3PO_4 and 0.165 M NaOH. Regarding Oxi-RPLIF, suitable conditions to employ this test-reaction would be RhB concentration up to 4 $mg·L^{-1}$, 2 % H_2O_2 (wt./v) and 0.010 M aqueous solution of Fe^{2+} (as $FeSO_4$, for economic benefit).

In AB-RPLIF method conducted in T-Jets mixers, the streams are initially clear fluids, and the reaction is assessed from the appearance of tracer. This is associated with the increase of its intensity of emission, giving a clear visualisation of the chemical reaction and the generation of the interfacial area between the two fluid streams. This feature is particularly useful in chaotic flow regimes where mixing occurs by interfacial area generation (Ottino et al., 1979). On the other hand, in the Oxi-RPLIF method, the streams are initially dyed with a tracer and reaction is assessed from the vanishing of tracer and then the decrease of its emission intensity. So, this method also enables to assess the chemical reaction rate throughout the mixing chamber. However, this method has the disadvantage of the formation of an undesirable iron sludge and more frequent gas bubbles during the experiments. Moreover, the Oxi-RPLIF method is also fivefold more expensive than AB-RPLIF, when using analytical grade reagents.

This work adapts and improves two reactive methods for the visualization of micromixing in large throughput continuous reactors. The two methods were demonstrated as efficient, safe, and cost effective for mixing visulaization.

Acknowledgments: The authors acknowledge FCT – Fundação para a Ciência e a Tecnologia, I.P. for the financial support through project PTDC/QEQ-FTT/0041/2014 - 2D Mixing Devices - Fundamental Study and Applications of the Inversion of the Turbulent Energy Cascade. Thanks also due to FCT/MCTES for the financial support to CESAM (UIDP/50017/2020 + UIDB/50017/2020 + LA/P/0094/2020), through national funds. This work was also financially supported by: LA/P/0045/2020 (ALiCE); UIDB/50020/2020 and UIDP/50020/2020 (LSRE-LCM), funded by national funds through FCT/MCTES (PIDDAC); by POCI-01-0145-FEDER-016851 and POCI-01-0145-FEDER-030445 – funded by FEDER funds - Programa Operacional Competitividade e Internacionalização (POCI) – and by national funds through FCT - Fundação para a Ciência e a Tecnologia I.P; M.S.C.A. Brito acknowledges her FCT scholarship PD/BD/135060/2017.

References

[1] Z. Liu, Y. Cheng, Y. Jin. *Chemical Engineering Journal*, **2009**, *150*(2), 536-543

[2] A. Lehwald, D. Thévenin, K. Zähringer. *Experiments in Fluids*, **2010**, *48*(*5*), 823-836
[3] J. Cheng, X. Feng, D. Cheng, C. Yang. *Chinese Journal of Chemical Engineering*, **2012**, *20*(*1*), 178-190
[4] P. Nadeau, D. Berk, R.J. Munz. *Chemical Engineering Science*, **1996**, *51*(*11*), 2607-2612
[5] M. Buchmann, D. Mewes. *The Canadian Journal of Chemical Engineering*, **1998**, *76*(*3*), 626-630
[6] M. Buchmann, D. Mewes. *Chemical Engineering Journal*, **2000**, *77*, 3-9
[7] J. Baldyga, J.R. Bourne, *Turbulent mixing and chemical reactions*. First Edition ed. 1999: John Wiley and Sons.
[8] M. Jasińska. *Chemical and Process Engineering*, **2015**, *36*,
[9] C.F. Dewey, Jr. *Qualitative and quantitative flow field visualization utilizing laser-induced fluorescence*. in *Applications of Non-intrusive Instrumentation in Fluid Flow Research*. 1976.
[10] K. Owen. *Simultaneous laser measurements of instantaneous velocity and concentration in turbulent mixing flows*. in *Applications of non-intrusive instrumentation in fluid flow research*. 1976.
[11] H.T. Liu, J.T. Lin, D.P. Delisi, F.A. Robben. *Application of a fluorescence technique to dye-concentration measurements in a turbulent jet*. in *Symposium on Flow Measurement in Open Channels and Closed Conduits*. 1977.
[12] D.A. Walker. *Journal of Physics E: Scientific Instruments*, **1987**, *20*(*2*), 217-224
[13] M. Bruchhausen, F. Guillard, F. Lemoine. *Experiments in Fluids*, **2005**, *38*(*1*), 123-131
[14] Y. Hu, Z. Liu, J. Yang, Y. Jin, Y. Cheng. *Chemical Engineering Science*, **2010**, *65*, 4511-4518
[15] D.R. Webster, P.J.W. Roberts, L. Ra'ad. *Experiments in Fluids*, **2001**, *30*(*1*), 65-72
[16] L. Milton-McGurk, N. Williamson, S.W. Armfield, M.P. Kirkpatrick. *International Journal of Heat and Fluid Flow*, **2020**, *82*, 108561
[17] L.A. Melton, C.W. Lipp. *Experiments in Fluids*, **2003**, *35*(*4*), 310-316
[18] J. Sakakibara, K. Hishida, M. Maeda. *Experiments in Fluids*, **1993**, *16*(*2*), 82-96
[19] N. Kuzkova, O. Popenko, A. Yakunov. *International Journal of Biomedical Imaging*, **2014**, *2014*, 243564
[20] L.E. Jardón-Pérez, A.M. Amaro-Villeda, G. Trápaga-Martínez, C. González-Rivera, M.A. Ramírez-Argáez. *Metallurgical and Materials Transactions B*, **2020**, *51*(*6*), 2510-2521
[21] A. Eltayeb, S. Tan, Z. Qi, A.A. Ala, N.M. Ahmed. *Annals of Nuclear Energy*, **2019**, *128*, 190-202
[22] X. Du, X. Duan, C. Yang. *Industrial & Engineering Chemistry Research*, **2019**, *58*(*47*), 21785-21796
[23] Z. Wang, J. Chen, X. Feng, Z.-S. Mao, C. Yang. *Chemical Engineering Science*, **2021**, *233*, 116401
[24] Z. Rida, S. Cazin, F. Lamadie, D. Dherbécourt, S. Charton, E. Climent. *Experiments in Fluids*, **2019**, *60*(*4*), 61
[25] J. Fitschen, S. Hofmann, J. Wutz, A.v. Kameke, M. Hoffmann, T. Wucherpfennig, M. Schlüter. *Chemical Engineering Science: X*, **2021**, *10*, 100098
[26] G. Rodriguez, M. Micheletti, A. Ducci. *Chemical Engineering Research and Design*, **2018**, *132*, 890-901
[27] A. Eltayeb, S. Tan, A.A. Ala, Q. Zhang. *Progress in Nuclear Energy*, **2021**, *131*, 103558
[28] X. Duan, X. Feng, Z.-S. Mao, C. Yang. *Chemical Engineering Journal*, **2019**, *360*, 1177-1187
[29] M. Taghavi, J. Moghaddas. *Chemical Engineering Research and Design*, **2019**, *151*, 190-206
[30] Y. Hu, W. Wang, T. Shao, J. Yang, Y. Cheng. *Chemical Engineering Research and Design*, **2012**, *90*(*4*), 524-533
[31] J.R. Bourne. *Organic Process Research & Development*, **2003**, *7*(*4*), 471-508
[32] J.R. Bourne, O.M. Kut, J. Lenzner, H. Maire. *Industrial & Engineering Chemistry Research*, **1990**, *29*(*9*), 1761-1765
[33] M. Nunes, R. Santos, M. Dias, J.C. Lopes. *Chemical Engineering Science, 74, 276-286 (2012)*, **2012**, *74*,
[34] T. Meyer, P.A. Fleury, A. Renken, J. Darbellay, P. Larpin. *Chemical Engineering and Processing: Process Intensification*, **1992**, *31*(*5*), 307-310
[35] J.R. Bourne, F. Kozicki. *Chemical Engineering Science*, **1977**, (*32*), 1538-1539
[36] K. Hecht, A. Koelbl, M. Kraut, K. Schubert. *Chemical Engineering & Technology*, **2008**, *31*, 1176-1181
[37] P.M. Oates, C.F. Harvey. *Experiments in Fluids*, **2006**, *41*(*5*), 673-683
[38] P. Zhang, S.L. DeVries, A. Dathe, A.C. Bagtzoglou. *Environmental Science & Technology*, **2009**, *43*(*16*), 6283-6288
[39] O. Akiti. *Turbulent mixing and chemical reaction in baffled stirred tank reactors : a comparison between experiments and a novel micromixing-based computational fluid dynamics model*. 2000.
[40] J. Baldyga, M. Henczka, L. Makowski. *Chemical Engineering Research and Design*, **2001**, *79*(*8*), 895-900
[41] J. Bałdyga, J.R. Bourne, S.J. Hearn. *Chemical Engineering Science*, **1997**, *52*(*4*), 457-466
[42] J.R. Bourne, S. Yu. *Industrial & Engineering Chemistry Research*, **1994**, *33*(*1*), 41-55
[43] J. Baldyga, J.R. Bourne. *Chemical Engineering Science*, **1990**, *45*(*4*), 907-916
[44] W.S. Tolgyesi. *Canadian Journal of Chemistry*, **1964**, (*43*), 345-365
[45] J. Baldyga, M. Jasinska, J. Trendowska, W. Tadeusiak, M. Cooke, A. Kowalski. *Application of test reactions to study micromixing and mass transfer in chemical apparatus*. 2012.
[46] M.C. Fournier, L. Falk, J. Villermaux. *Chemical Engineering Science*, **1996**, *51*(*22*), 5053-5064
[47] P. Guichardon, L. Falk. *Chemical Engineering Science*, **2000**, *55*(*19*), 4233-4243
[48] A. Ghanem, T. Lemenand, D. Della Valle, H. Peerhossaini. *Chemical Engineering Research and Design*, **2014**, *92*(*2*), 205-228
[49] J. Baldyga, J.R. Bourne, B. Walker. **1998**, *76*(*3*), 641-649
[50] M. Faes, B. Glasmacher. *Chemical Engineering Science*, **2008**, *63*(*19*), 4649-4655
[51] K. Kling, D. Mewes. *Chemical Engineering Science*, **2004**, *59*, 1523-1528
[52] P.M. Wheat, J.D. Posner. **2009**, *21*(*3*), 037101
[53] A. Lehwald, S. Jenrich, D. Thévenin, K. Zahrinque, *Experimental investigation of macro- and micro-mixing in a reactive turbulent channel flow*, in *16th International Symposium on Applications of Laser Techniques to Fluid Mechanics*. 2012: Lisbon. p. 1-10.

[54] A. Lehwald, D. Thévenin, K. Zähringer, *Simultaneous two-tracer-Laser-induced fluorescence and particle image velocimetry for the investigation of macro-and micro-mixing in a static mixer*, in *15th International Symposium on Applications of Laser Techniques to Fluid Mechanics*. 2010: Lisbon.
[55] A. Fall, O. Lecoq, R. David. *Chemical Engineering Research and Design*, **2001**, *79*(*8*), 876-882
[56] G. Rule, W.R. Seitz. *Clin Chem*, **1979**, *25*(*9*), 1635-8
[57] M. Shamsipur, M.J. Chaichi, A.R. Karami. *Spectrochimica Acta Part A: Molecular and Biomolecular Spectroscopy*, **2003**, *59*(*3*), 511-517
[58] T. Jonsson, K. Irgum. *Analytica Chimica Acta*, **1999**, *400*(*1*), 257-264
[59] P.S. Karasso, M.G. Mungal. *Experiments in Fluids*, **1997**, *23*(*5*), 382-387
[60] M. Mortensen, W. Orciuch, M. Bouaifi, B. Andersson. *Chemical Engineering Research and Design*, **2004**, *82*(*3*), 357-363
[61] M.A. Sultan, C.P. Fonte, M.M. Dias, J.C.B. Lopes, R.J. Santos. *Chemical Engineering Science*, **2012**,
[62] J. Coppeta, C. Rogers. *Experiments in Fluids*, **1998**, *25*(*1*), 1-15
[63] M.M. Koochesfahani. *Experiments on turbulent mixing and chemical reactions in a liquid mixing layer.*, in Aeronautics Department. 1984, California Institute of Technology., PhD.
[64] M.M. Koochesfahani, P.E. Dimotakis. *Journal of Fluid Mechanics*, **1986**, *170*, 83-112
[65] L. Kola, S. Amataj. *Macedonina Journal of Chemistry and Chemical Engineering* **2006**, *25*(*2*), 107-112
[66] D. Bothe, C. Stemich, H.-J. Warnecke. *Computers & Chemical Engineering*, **2008**, *32*(*1*), 108-114
[67] M. Hoffmann, M. Schlüter, N. Räbiger. *Chemical Engineering Science*, **2006**, *61*(*9*), 2968-2976
[68] A. Soleymani, E. Kolehmainen, I. Turunen. *Chemical Engineering Journal*, **2008**, *135*, S219-S228
[69] A. Soleymani, H. Yousefi, I. Turunen. *Chemical Engineering Science*, **2008**, *63*(*21*), 5291-5297
[70] M.A. Sultan, K. Krupa, C.P. Fonte, M.I. Nunes, M.M. Dias, J.C.B. Lopes, R.J. Santos. **2013**, *36*(*2*), 323-331
[71] M.A. Sultan, S.L. Pardilhó, M.S.C.A. Brito, C.P. Fonte, M.M. Dias, J.C.B. Lopes, R.J. Santos. *Chemical Engineering & Technology*, **2019**, *42*(*1*), 119-128
[72] J.P. Crimaldi. *Experiments in Fluids*, **2008**, *44*(*6*), 851-863